Electronic Supplementary Material (ESI)

for ***Dalton Transactions***

Semiquantitative studies on the correlations between the electrostatic potential of a single Dy^{III} ion and its energy barrier in the containing-Dy^{III} single molecule magnets

Jia-Rong Jiang,‡ Yu-Jie Zhu,‡ Wei-Nan Li, Yang Zhou and Hui-Sheng Wang*

School of Chemistry and Environmental Engineering, Wuhan Institute of Technology, Key Laboratory of Novel Reactor and Green Chemical Technology of Hubei Province, Key Laboratory for Green Chemical Process of Ministry of Education, Wuhan 430074, P. R. China.

‡J.R.J. and Y.J.Z. contributed equally as cofirst authors.

Corresponding Author

*Email: wangch198201@163.com (H.-S. W.).

Contents

I. General information from references

Table S1. The structural and magnetic parameters for the selected Mn^{III}-Dy complexes with SMM behavior.

Complexes	Topologies	Geometries of Dy	*Complete profile for χ''*	U_{eff} (K)	Ref.
$[Mn_{21}DyO_{20}(OH)_2(Bu^tCO_2)_{20}(HCO_2)_4(NO_3)_3(H_2O)_7]$	Not reported	Not reported	yes	74[a]	S1
$[Mn_{12}Dy_6O_7(OH)_{10}(OAc)_{14}(mpea)_8]\cdot 20H_2O\cdot 4MeOH$	Not reported	Not reported	yes	~35[a]	S2
$TBA_2[Mn_4Dy_2(teaH)_4(N_3)_{12}]$	Not reported	MSAP	yes	~44[a]	S3
$[Mn_5Dy_4(O)_6(mdea)_2(mdeaH)_2(piv)_6(NO_3)_4(H_2O)_2]$	Not reported	TTP	yes	~39[a]	S4
$[Mn^{III}_2Dy^{III}_2(\mu_3\text{-}OH)_2(p\text{-}Me\text{-}PhCO_2)_6(L^a)_2]^*$	Butterfly	SCSAP	yes	~19[a]	S5
$[Mn^{III}_2Dy_3(L^bH)_4(NO_3)(HOCH_3)]ClO_4\cdot NO_3$	Open-book	TDDC and SAP	partial	13[a]	S6
$[Mn_{26}Dy_6O_{16}(OH)_{12}(O_2CCHMe_2)_{42}]$	Not reported	TDDC and MSAP	not reported	46[a]	S7
$[Mn^{III}(\mu\text{-}L^c)(\mu\text{-}OMe)(NO_3)Dy^{III}(NO_3)_2(MeOH)]^{**}$	Not reported	Not reported	not	/	S8
$[Mn_2Dy_2(L^dH)_4(\mu\text{-}OAc)_2](NO_3)_2\cdot 2CH_3OH\cdot 3H_2O$	Arch-like	Not reported	not	~24[a]	S9
$[Mn^{III}_2Dy_2(OMe)_2(O_2CMe)_6(naph)_2]$	Linearity	SAP	not	/	S10
$[Mn^{IV}Mn^{III}_2Dy^{III}_2O_2(benz)_4(mdea)_3(NO_3)_2(MeOH)]^{***}$	Trigonal bipyramid	MSAP	not	/	S11
$[Mn^{II}Mn^{III}_2Dy^{III}_4(mosao)_2(mosaoH)_4(piv)_4(mdea)_4]$	Not reported	Not reported	not	~9[a]	S12
$[Mn^{III}_4Dy^{III}(HL^e)_4\{(py)_2CO_2\}_2Cl_2](OH)$	Tetrahedron	cube	not	7.9[b]	S13
$[Mn_4Dy_2O_2\{(py)_2CO_2\}_4(NO_3)_4(EtCO_2)_2(H_2O)_3(MeOH)]$	Cross-shape	TCTP	not	/	S14
$(NHEt_3)[Mn_4Dy_5O_2(OH)_4(NO_3)_4(saph)_8(H_2O)_4]$	Not reported	Not reported	not	/	S15
$[Mn^{III}_4Dy^{III}_4(OH)_4(N_3)_4(O_2CBu^t)_8(t\text{-}bdea)_4]\cdot solv$	Square-in-square	SAP	not	/	S16
$[Mn_6Dy_2(OH)_4(O)(Ac)_4(H_2O)_2(L^f)_6]\cdot NO_3\cdot OH$	Sandwich	TCTP	not	~15[b]	S17
$[Mn^{III}_6Dy^{III}_6(OH)_7(H_2O)_3(O_2CPh)_{11}(L^g)_3(HL^g)_4(NO_3)]$	Not reported	SCSAP	not	/	S18
$[Mn^{III}_4Mn^{II}_2Dy^{III}_{10}O_4(OH)_{12}(OAc)_{16}(L^h)_4(HL^h)_2(EtOH)_2]$	Squarelike	SAP and CTPR	not	~11[a]	S19
$[Mn_7Dy_2(O)_6(OMe)_2(OH)(piv)_8(dea)_2(MeOH)_2(H_2O)_2]$	Not reported	BTPR	not	~10[a]	S20
$[Mn_8Dy_2O_2(OH)_2\{(py)_2CO_2\}_4(teaH)_4(CH_3COO)_6]\cdot solv$	Not reported	MFF	not	/	S21
$[Mn^{III}_8Dy^{III}_8(mdea)_{16}(o\text{-}tol)_8(NO_3)_8]^{****}$	Wheels	TDDC	not	/	S22
$[Mn^{III}_{12}Mn^{II}_6Dy^{III}(O)_8(Cl)_{6.5}(N_3)_{1.5}(HL^i)_{12}(MeOH)_6]Cl_3$	Supertetrahedron	Not reported	not	/	S23

TDDC = trigonal dodecahedron, MSAP = monocapped square antiprism, TCTP = tricapped trigonal, Prism, SAP = square antiprism, SCSAP = spherical capped square antiprism, MFF = muffin, TTP = triaugmented triangular prism, BTPR = biaugmented trigonal prism, CTPR = capped trigonal prism; [a] the values of the effective energy barrier (U_{eff}) were obtained by employing Arrhenius law ($\tau = \tau_0 \exp(U_{eff}/kT)$), [b] the values of the energy barrier (E_a) were obtained by the equation of $\ln(\chi''/\chi') = \ln(\omega\tau_0) + E_a/k_BT$; H_2mpea = 2-hydroxy-3-((2-hydroxyethylimino)methyl)-5-methylbenzaldehyde, $teaH_3$ = triethanolamine, $mdeaH_2$ = *N*-methyldiethanolamine, pivH = pivalic acid, *p*-Me-$PhCO_2H$ = 4-methylbenzoic acid, H_2L^a = 2,2'-((pyridin-2-ylmethyl)azanediyl)bis(ethan-1-ol), L^bH_4 = (*E*)-2,2'-(2-hydroxy-3-((2-hydroxyphenylimino)methyl)-5-methylbenzylazanediyl)-diethanol, H_2L^c = 6,6'-{(2-(1-morpholyl)ethylazanediyl)bis-(methylene)}bis(2-methoxy-4-methylphenol), L^dH_3 = 2,2'-(2-hydroxy-3-methoxy-5-methylbenzylazanediyl)diethanol, $naphH_2$ = *N*-naphthalidene-*o*-aminophenol, benz(H) = benzoic acid, $mosaoH_2$ = 3-methyloxysalicylaldoxime, H_3L^e = 2-((2-hydroxybenzylidene)amino)propane-1,3-diol, $(py)_2C(OH)_2$ = the gem-diol form of 2,2′-dipyridyl ketone), $saphH_2$ = *N*-salicylidene-*o*-aminophenol, *t*-$bdeaH_2$ = *t*-butyldiethanolamine, H_2L^f = the condensation reactions with *o*-vanillin and *R*-/*S*-2-phenylglycinol, H_3L^g = 2-(β-naphthalideneamino)-2-hydroxymethyl-1-propanol, H_2L^h = 4-bromo-2-[(2-hydroxypropylimino)methyl]phenol, H_2dea = diethanolamine, *o*-tol = *ortho*-toluic acid, H_3L^i = 2,6-bis-(hydroxymethyl)-4-methylphenol.

The calculated energy barrier (U_{cal}) by *ab initio* calculations: *$U_{cal,Dy1} = U_{cal,Dy2} = 50.2$ cm^{-1}; ***$U_{cal,Dy1} = 53$ cm^{-1}; ***$U_{cal,Dy1} = 20.5$ cm^{-1}, $U_{cal,Dy2} = 52.3$ cm^{-1}; **** $U_{cal,Dy1} = 65.1$ cm^{-1}, $U_{cal,Dy2} = 90.7$ cm^{-1}.

II. Experimental part

EXPERIMENTAL SECTION

All chemical reagents were obtained from commercial sources and used without further purification. All reactions were carried out under aerobic conditions. The 2-methoxy-6-[(*Z*)-(1*H*-1,2,4-triazol-3-ylimino)methyl]phenol ligand (H_2L) was prepared by the already reported method.[S24]

Synthesis of $[Mn^{III}_5Dy^{III}_3(NO_3)(OCH_3)(L)_4(L')_2(tea)(teaH)_4]OH\cdot 3CH_3OH\cdot 2H_2O$ (1)

A mixture of $MnCl_2\cdot 4H_2O$ (0.0396 g, 0.2 mmol), $Dy(NO_3)_3\cdot 6H_2O$ (0.0457 g, 0.1 mmol), H_2L ligand (0.0436 g, 0.2 mmol), triethanolamine (0.0301 g, 0.2 mmol), and tetramethylammonium hydroxide pentahydrate (0.1449 g, 0.8 mmol) dissolved in the mixture of CH_3OH and DMF (15 mL, the volume ratio of CH_3OH: DMF = 14:1), which was stirred at room temperature for 25 min. The black clear solution was obtained by filtration. After 3 weeks, red-brown block-shaped crystals suitable for single-crystal X-ray diffraction analysis were isolated from the slow evaporation of the solvent, which was washed with a small amount of CH_3OH and dried in air. The yield was 0.0110 g (9.84% based on Mn salt or 11.82% based on Dy salts). Three CH_3OH and one H_2O solvent molecules in the crystal lattice were lost when the sample of **1** was dried. Anal. Calcd for $C_{87}H_{116}Dy_3Mn_5N_{22}O_{35}$ (*M*r = 2792.17): C, 37.42%; H, 4.19%; N%, 11.04%. Found: C, 37.60%; H, 4.12%; N, 10.95%. Selected IR (Figure S1, KBr, cm^{-1}, s, m, and w stand for strong, medium, and weak, respectively): 3389(s), 2850(s), 1659(s), 1602(s), 1545(s), 1471(s), 1433(s), 1366(s), 1291(s), 1248(s), 1215(s), 1072(s), 972(m), 912(m), 862(m), 742(m), 638(m), 503.91(m).

Crystal Structure Determination

Single-crystal X-ray diffraction data were collected at 150(2) K for **1** on a Bruker Smart CCD diffractometer with graphite-monochrome-mated GaKα (λ = 1.34138 Å) radiation in a ω-scan mode. The collected data were reduced using the software package SAINT,[S25] and a semiempirical absorption correction was applied to the intensity data using the SADABS program.[S26] The crystal structure of **1** was solved by employing direct methods, all non-hydrogen atoms were refined anisotropically by least squares on F^2 using the SHELXL-2014 program,[S27] and all H atoms were placed at calculated positions and isotropically fixed using the riding model. Some solvent molecules in **1** cannot be properly modeled, so the contributions were subtracted by the SQUEEZE command as implemented in PLATON.[S28] The crystallographic data and structure refinement parameters are summarized in Table S2. Selected bond lengths and angles for **1** are given in Table S3.

Physical measurements

The crystals of **1** were filtrated from its mother solutions, washed three times with CH_3OH, and dried in the air overnight. The collected powder sample of **1** was measured for infrared spectra (IR), elemental analysis, and magnetic properties. IR spectral data were measured on a Nexus 670 FT-IR spectrometer using KBr pellets in the range of 400 to 4000 cm^{-1}. Elemental analysis (C, H, and N) of **1** was recorded with an Elementar Vario EL cube. The magnetic measurements of the crystalline

sample were performed on a Quantum Design MPMS-XL7 SQUID magnetometer. The direct current (dc) magnetic susceptibility measurements were carried out under an applied field of 1000 Oe from 2.0 to 300 K. The magnetization (*M*) measurements were performed in the range of 0-7 T and 2.0-5.0 K. The alternating current (ac) magnetic susceptibilities were collected under a zero dc field or under different applied dc fields with a 5 Oe ac oscillating field. The oscillation frequencies range from 1 Hz to 999 Hz. The diamagnetic corrections for **1** were estimated using Pascal's constants,[S29] and the magnetic data were corrected for diamagnetic contributions from the sample holder.

III. Structural part

Table S2. Crystal data and structure refinement parameters for complexes **1**.

Complex	Complex **1**
Empirical formula	$C_{90}H_{130}Dy_3Mn_5N_{22}O_{39}$
Formula weight	2906.35
Temperature/K	150(2)
Crystal color	dark brown
Crystal system	triclinic
Space group	$P\bar{1}$
a (Å)	18.3119(9)
b (Å)	19.3604(9)
c (Å))	24.2054(13)
α (°)	93.079(2)
β (°)	108.015(2)
γ (°)	106.125(2)
Volume/Å^3	7747.6(7)
Z	2
ρ_{calc} (g/cm^3)	1.246
μ(Ga Kα)/mm^{-1}	9.962
F(000)	2918
Crystal size/mm^3	0.15 × 0.12 × 0.10
Radiation	GaKα (λ = 1.34138)
θ range/°	3.3447-56.9075
Index ranges	$-22 \leq h \leq 22$, $-24 \leq k \leq 23$, $-30 \leq l \leq 30$
Reflections collected	119605
Unique reflections [R_{int}]	31748 [R_{int} = 0.0802]
Reflections with $I > 2\sigma(I)$	21152
Goodness-of-fit on F^2	1.093
Final *R* indexes [$I >= 2\sigma(I)$] [a,b]	R_1 = 0.0638, wR_2 = 0.1542
Final *R* indexes [all data]	R_1 = 0.0951, wR_2 = 0.1701
S (all data)	1.097

[a] $R_1 = \Sigma(||F_o| - |F_c||)/\Sigma|F_o|$.

[b] $wR_2 = [\Sigma[w(F_o^2 - F_c^2)^2]/\Sigma[w(F_o^2)^2]]^{0.5}$, $w = 1/[\sigma^2(F_o^2) + [(ap)^2 + bp]$, where $p = [\max(F_o^2, 0) + 2F_c^2]/3$.

Table S3. Selected bond lengths (Å) and angles (°) for **1**.

Selected bond lengths for **1**					
Dy1-O15	2.294(4)	Dy3-O29	2.321(5)	Mn2-N11	2.257(5)
Dy1-O33	2.322(4)	Dy3-O25	2.350(5)	Mn3-O9	1.901(5)
Dy1-O30	2.376(4)	Dy3-O27	2.406(5)	Mn3-O23	1.903(4)
Dy1-O16	2.385(4)	Dy3-O28	2.421(4)	Mn3-O20	1.906(5)
Dy1-O17	2.430(4)	Dy3-O26	2.488(6)	Mn3-O5	1.932(4)
Dy1-O31	2.429(4)	Dy3-N21	2.582(6)	Mn3-N9	2.275(5)
Dy1-N2	2.565(5)	Dy3-N14	2.600(6)	Mn3-O10	2.278(5)
Dy1-N6	2.610(5)	Dy3-N20	2.612(6)	Mn4-O24	1.904(5)
Dy1-N17	2.650(5)	Mn1-O3	1.893(5)	Mn4-O16	1.908(5)
Dy2-O23	2.301(5)	Mn1-O33	1.908(4)	Mn4-O27	1.944(5)
Dy2-O21	2.327(4)	Mn1-O1	1.917(5)	Mn4-N3	2.025(6)
Dy2-O18	2.337(4)	Mn1-O15	1.938(4)	Mn4-O31	2.251(4)
Dy2-O20	2.395(4)	Mn1-N5	2.269(6)	Mn4-N15	2.264(6)
Dy2-O22	2.435(4)	Mn1-N1	2.269(6)	Mn5-O7	1.907(6)
Dy2-O19	2.474(5)	Mn2-O17	1.881(4)	Mn5-O25	1.911(5)
Dy2-N18	2.598(6)	Mn2-O21	1.912(4)	Mn5-O29	1.918(5)
Dy2-N19	2.603(6)	Mn2-O18	1.922(4)	Mn5-O12	1.925(7)
Dy2-N10	2.651(5)	Mn2-N7	2.015(6)	Mn5-O13	2.236(9)
Dy3-O24	2.306(4)	Mn2-O30	2.216(4)	Mn5-N13	2.247(8)
Selected bond angles for **1**					
O15-Dy1-N17	67.76(16)	N21-Dy3-N20	140.1(2)	O9-Mn3-N9	86.9(2)
O33-Dy1-N17	135.02(16)	N14-Dy3-N20	97.3(2)	O23-Mn3-N9	104.82(19)
O30-Dy1-N17	131.24(14)	O3-Mn1-O33	94.79(19)	O20-Mn3-N9	87.6(2)
O16-Dy1-N17	67.17(17)	O3-Mn1-O1	89.7(2)	O5-Mn3-N9	83.08(18)
O17-Dy1-N17	66.58(14)	O33-Mn1-O1	174.4(2)	O24-Mn4-N15	84.7(2)
O23-Dy2-O21	86.56(15)	O3-Mn1-O15	175.5(2)	O16-Mn4-N15	102.3(2)
O23-Dy2-O18	143.78(17)	O33-Mn1-O15	84.28(17)	O27-Mn4-N15	82.2(2)
O21-Dy2-O18	66.06(14)	O18-Mn2-N7	173.7(2)	N3-Mn4-N15	95.7(2)
O23-Dy2-O20	63.71(15)	O17-Mn2-O30	78.92(15)	O31-Mn4-N15	176.3(2)
O21-Dy2-O20	137.31(16)	O21-Mn2-O30	93.15(16)	O25-Mn5-O12	172.5(3)
O27-Dy3-N20	132.77(18)	O18-Mn2-O30	97.61(17)	O29-Mn5-O12	93.1(3)
O28-Dy3-N20	85.06(18)	N7-Mn2-O30	87.85(19)	O7-Mn5-O13	86.1(3)
O26-Dy3-N20	67.0(2)	O20-Mn3-O5	93.33(19)	O25-Mn5-O13	96.8(3)

Table S4. Bond Valence Sum (BVS) calculations for determining the oxidation of the Mn in **1**.

Atom	+2	+3	+4
Mn1	3.57	3.29	3.23
Mn2	3.47	3.20	3.14
Mn3	3.45	3.18	3.12
Mn4	3.37	3.11	3.05
Mn5	3.50	3.23	3.17

Note: The values labeled by underline indicated that they are close to the assigned oxidation state of Mn atoms. In **1**, the oxidation states of five Mn atoms are all +3.

Table S5. Bond Valence Sum (BVS) calculations for determining the protonation levels of the O atoms in **1**.

Atoms	BVS values	Atoms	BVS values
O1	1.72	O18	2.02
O2	2.01	O19	1.19
O3	1.88	O20	1.94
O4	1.91	O21	2.07
O5	1.86	O22	1.31
O6	1.87	O23	2.13
O7	2.02	O24	2.08
O8	1.96	O25	2.12
O9	1.91	O26	1.18
O10	1.75	O27	1.83
O11	1.95	O28	1.26
O12	2.07	O29	2.00
O13	1.83	O30	1.84
O14	1.88	O31	1.72
O15	2.10	O32	1.60
O16	1.96	O33	2.10
O17	1.97		

Note: 1) The values of BVS calculations for O atoms in the 1.8-2.0, 1.0-1.2, and 0.2-0.4 ranges are indicative of non-, single- and double-protonation, respectively. 2) The O atoms with single-protonation were labeled by red.

Table S6. The possible geometries of Dy1 and its deviation parameters from each ideal polyhedron in **1**.

Point group	Geometry	Polyhedron	Dy1
D_{9h}	EP-9	Enneagon	36.594
C_{8v}	OPY-9	Octagonal pyramid	24.864
D_{7h}	HBPY-9	Heptagonal bipyramid	16.339
C_{3v}	JTC-9	Johnson triangular cupola (J3)	14.064
C_{4v}	JCCU-9	Capped cube (J8)	9.888
C_{4v}	CCU-9	Spherical-relaxed capped cube	8.776
C_{4v}	JCSAPR-9	Capped square antiprism (J10)	4.023
C_{4v}	CSAPR-9	Spherical capped square antiprism	3.183
D_{3h}	JTCTPR-9	Tricapped trigonal prism (J51）	5.716
D_{3h}	TCTPR-9	Spherical Tricapped trigonal prism	3.885
C_{3v}	JTDIC-9	Tridiminished icosahedron(J63)	9.924
C_{2v}	HH-9	Hula-hoop	8.330
C_s	MFF-9	Muffin	2.003

Note: The coordination geometry of Dy1 was labeled by red.

Table S7. The possible geometries of Dy2 and Dy3 as well as their deviation parameters from each ideal polyhedron in **1**.

Point group	Geometry	Polyhedron	Dy2	Dy3
D_{9h}	EP-9	Enneagon	36.072	35.722
C_{8v}	OPY-9	Octagonal pyramid	21.489	22.367
D_{7h}	HBPY-9	Heptagonal bipyramid	17.497	17.743
C_{3v}	JTC-9	Johnson triangular cupola (J3)	16.046	16.455
C_{4v}	JCCU-9	Capped cube (J8)	8.742	9.805
C_{4v}	CCU-9	Spherical-relaxed capped cube	6.940	8.208
C_{4v}	JCSAPR-9	Capped square antiprism (J10)	3.335	2.446
C_{4v}	CSAPR-9	Spherical capped square antiprism	1.915	1.693
D_{3h}	JTCTPR-9	Tricapped trigonal prism (J51）	3.586	3.683
D_{3h}	TCTPR-9	Spherical Tricapped trigonal prism	1.755	1.723
C_{3v}	JTDIC-9	Tridiminished icosahedron(J63)	12.294	13.039
C_{2v}	HH-9	Hula-hoop	8.682	8.701
C_s	MFF-9	Muffin	2.022	1.572

* The CShM values of the coordination geometries close to each other were labelled using blue.

Table S8. The distance (d, Å) and angle (°) information for the intramolecular and/or intermolecular hydrogen bonds in complexes **1**.

D-H···A	d(D-H)	d(H···A)	d(D···A)	∠(DHA)	Symmetry codes
O39-H39A···O27	0.85	2.09	2.937	178.6	
O38-H38A···O14$^{\#1}$	0.85	2.18	2.894	142.0	#1 = $x-1, y, z$
O38-H38B···O12$^{\#1}$	0.85	2.18	2.906	144.0	#1 = $x-1, y, z$
O37-H37B···O8$^{\#2}$	0.85	2.20	2.911	141.1	#2 = $x, y, z-1$
O37-H37A···O13$^{\#2}$	0.85	2.51	3.050	121.8	#2 = $x, y, z-1$
O37-H37A···O7$^{\#2}$	0.85	2.17	2.898	143.8	#2 = $x, y, z-1$
O36-H36···O34	0.85	1.89	2.741	175.4	
O35-H35A···O2	0.85	2.34	2.949	129.1	
O35-H35A···O1	0.85	2.38	3.199	163.1	
O34-H34A···O5	0.85	1.91	2.759	178.9	
O28-H28A···O32	0.85	1.80	2.594	154.3	
O26-H26A···O25	0.85	2.42	2.906	116.9	
O22-H22A···O32	0.85	1.89	2.670	151.5	
O19-H19A···O36	0.85	2.03	2.670	131.6	
O19-H19A···O20	0.85	2.40	2.910	119.5	

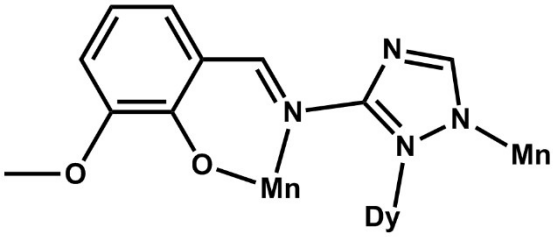

Coordination mode μ_3–κ^1-O,O':κ^1-N,N',N''

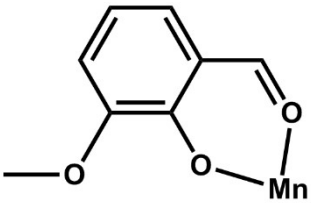

Coordination mode μ_1–κ^1-O,O'

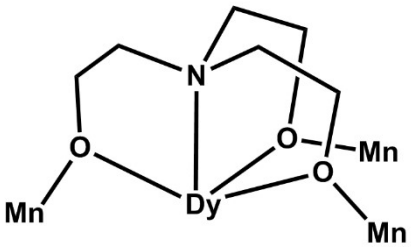

Coordination mode μ_4–κ^2-O,O',O'':κ^1-N

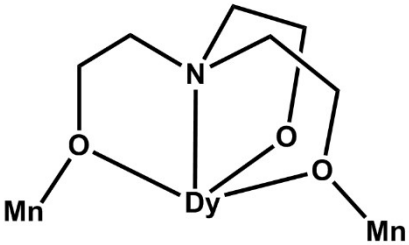

Coordination mode μ_3–κ^2-O,O':κ^1-O'':κ^1-N

Scheme S1. The coordination modes of L^{2-}, L'^{-}, tea^{3-}, and $teaH^{2-}$ in **1**.

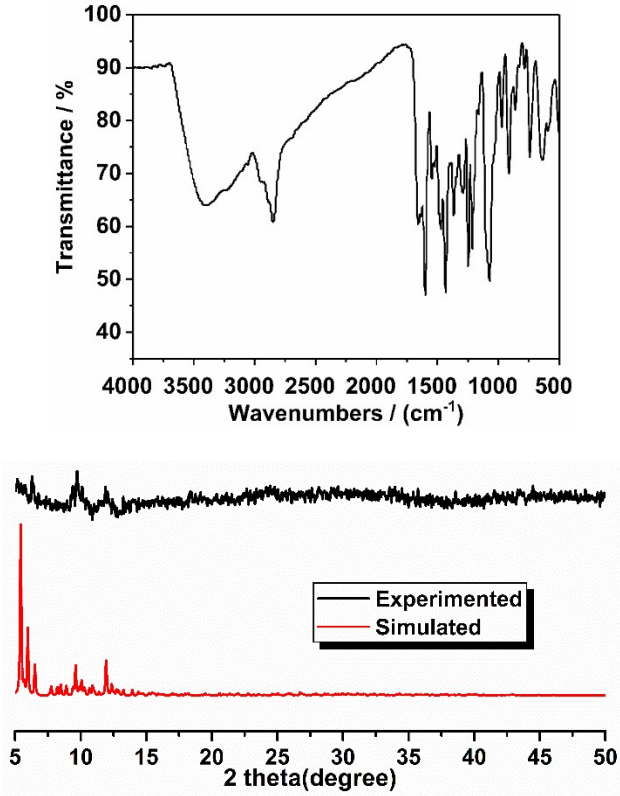

Figure S1. IR spectra (upper) and PXRD patterns (bottom) of **1**.

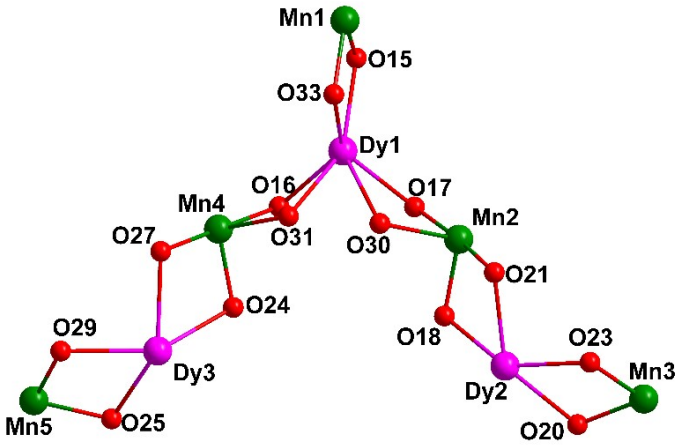

Figure S2. The topology of the metal core in **1**.

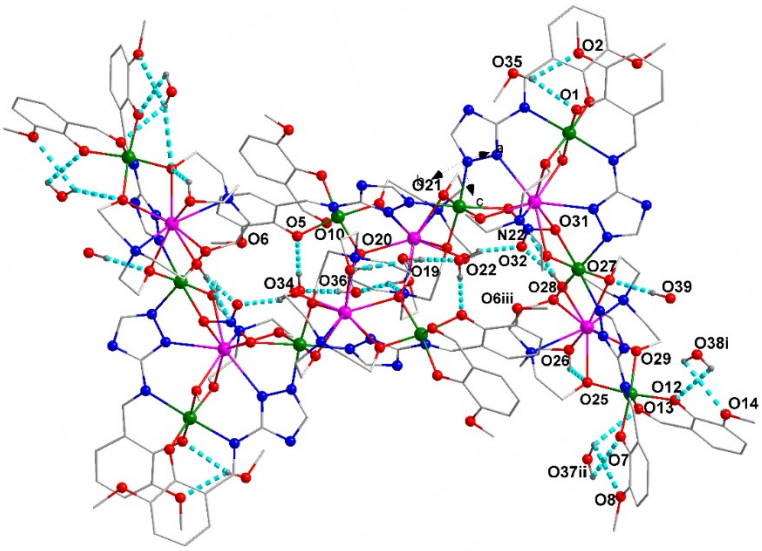

Figure S3. The hydrogen bond presented in the crystal of **1**.

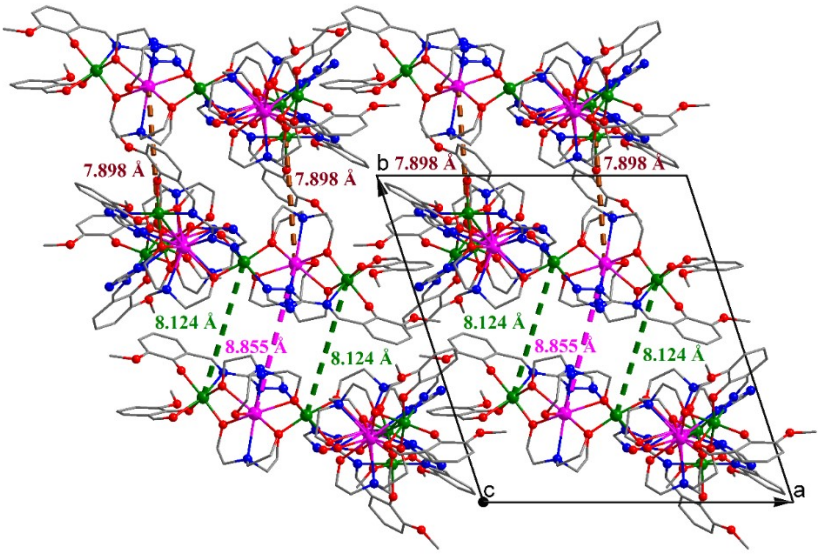

Figure S4. The shortest $Dy^{III}\cdots Dy^{III}$ (pink dashed lines), $Mn^{III}\cdots Mn^{III}$ (green dashed lines) and $Mn^{III}\cdots Dy^{III}$ (brown dashed lines) distances between the neighboring molecules of **1** in the packing diagram along with *c*-axis.

IV. Magnetic part

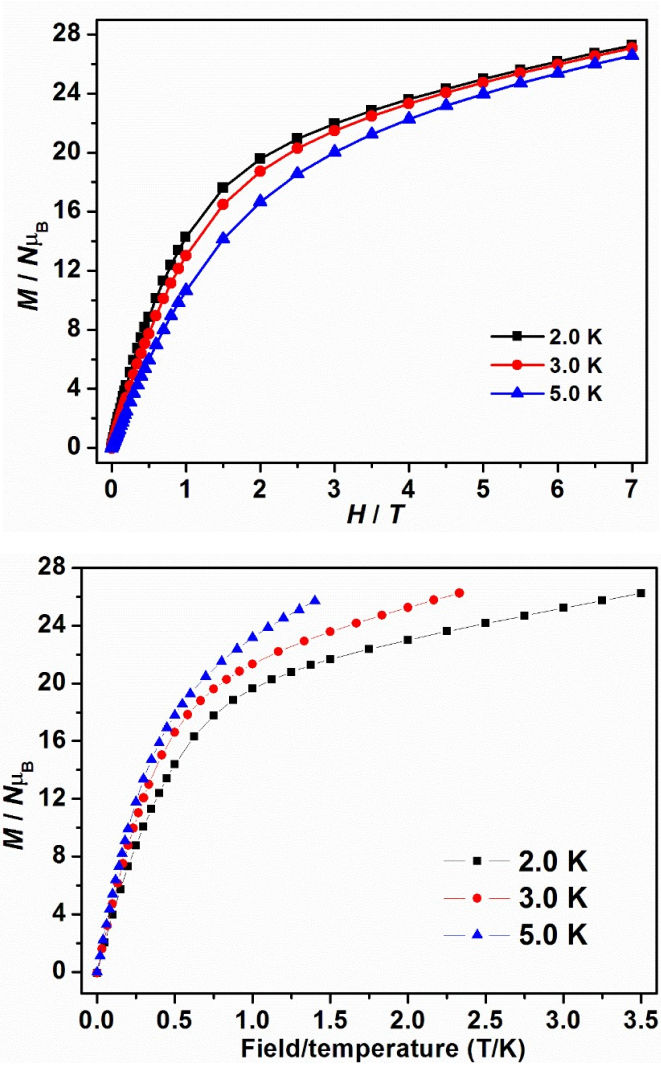

Figure S5. The plots of *M vs H* (top) and *M vs H/T* for **1**.

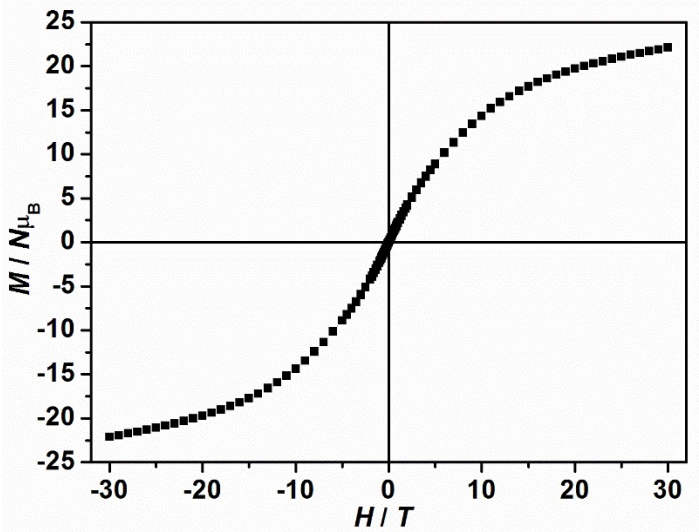

Figure S6. Hysteresis loops of **1** measured at 1.8 K (the field sweep rate is 0.02 T s^{-1}).

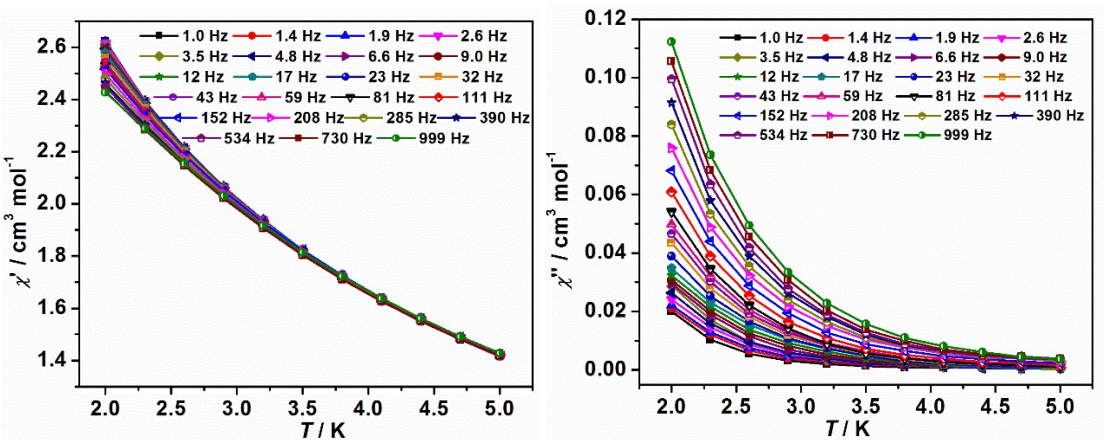

Figure S7. The plots of in-phase (χ') ac susceptibilities *vs*. T (left, T represents temperature) and out-of-phase ac susceptibilities (χ'') *vs*. T (right) of **1** mesured under a zero dc field.

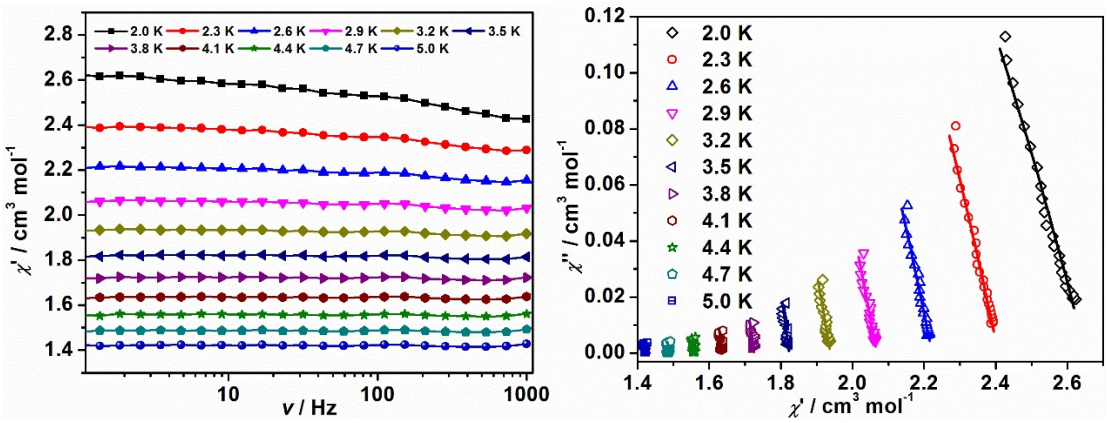

Figure S8. The plots of in-phase (χ') ac susceptibilities *vs*. ν (left, ν represents frequency) and Cole-Cole plots (right) of **1** mesured under a zero dc field. The solid lines in the right figure represent the fitted results by employing a single relaxation Debye model.

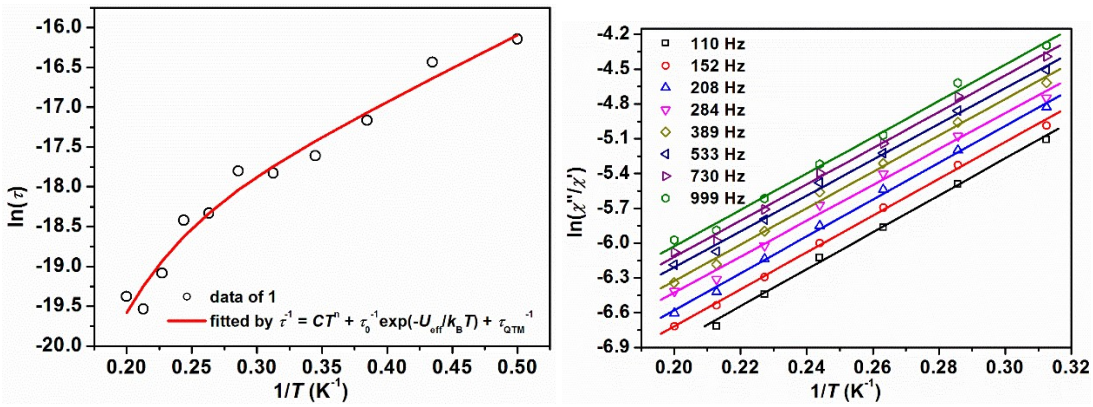

Figure S9. The plots of ln(τ) *vs*. T^{-1} (left) and ln(χ''/χ') *vs*. T^{-1} for **1** measured under a zero dc field. The red solid line in the left figure and the solid lines with different colors in the right figure represent the fitted results by $\tau^{-1} = CT^n + \tau_0^{-1}\exp(-U_{eff}/k_BT) + \tau_{QTM}^{-1}$ and by $\ln(\chi''/\chi') = \ln(\omega\tau_0) + U_{eff}/k_BT$, respectively.

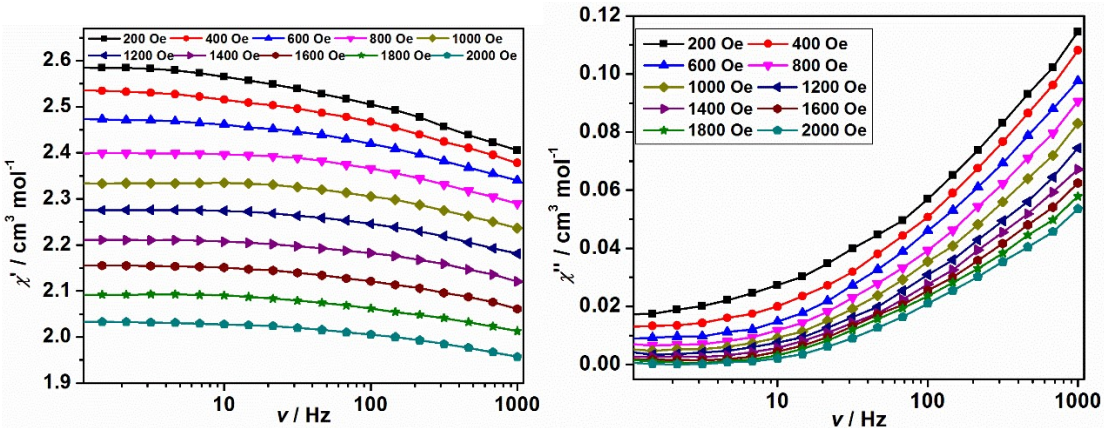

Figure S10. The plots of χ' *vs*. ν (left) and χ'' *vs*. ν (right) of **1** mesured under different dc fields.

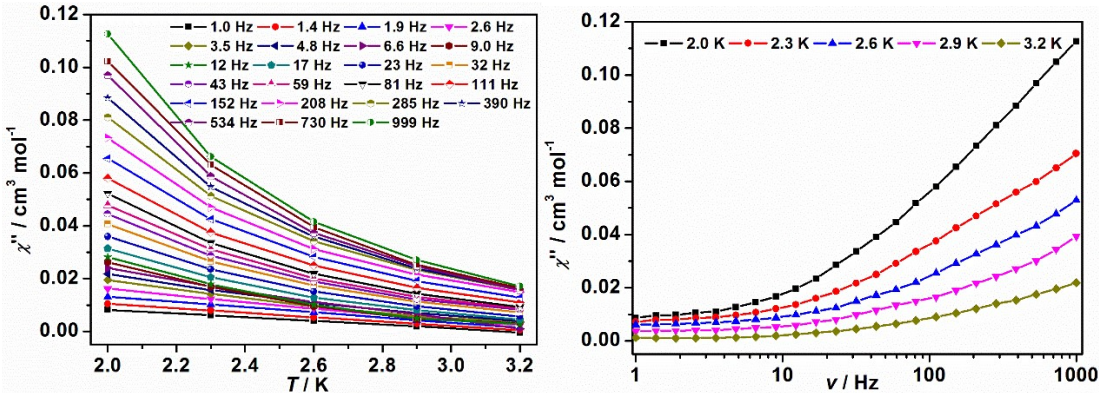

Figure S11. The plots of χ'' *vs*. T (left) and χ'' *vs*. ν (right) of **1** mesured under a 200 Oe dc field.

Table S9. Best fitted parameters obtained from the fits of the Cole-Cole plots of **1** under a zero Oe dc field by employing a single relaxation Debye model.

T (K)	χ_S	χ_T	τ (s)	α	Residual
2.0	2.6516E-13	2.6506	9.75731E-8	0.70027	8.40507E-4
2.3	5.41266E-13	2.40778	7.52628E-8	0.65177	6.77443E-4
2.6	3.78686E-13	2.22234	3.51262E-8	0.63453	5.30432E-4
2.9	5.13945E-13	2.06786	1.94241E-8	0.61294	4.60646E-4
3.2	1.0057E-12	1.93802	1.80759E-8	0.5823	4.13361E-4
3.5	3.74684E-13	1.82305	2.78228E-8	0.51357	3.97155E-4
3.8	4.76905E-13	1.7249	1.09378E-8	0.52	3.33538E-4
4.1	8.36163E-13	1.6365	1.06772E-8	0.48918	2.95299E-4
4.4	3.66983E-12	1.55833	4.67153E-9	0.49877	2.36341E-4
4.7	4.97033E-12	1.48687	3.28228E-9	0.48626	2.17527E-4
5	2.08795E-12	1.42193	4.09505E-9	0.46029	1.93754E-4

Table S10. The obtained parameters by employing the Bartolomé equation for fitting the magnetic data of **1** under a zero dc field.

Frequencies (Hz)	τ_0 (s)	E_a (K)	Frequencies (Hz)	τ_0 (s)	E_a (K)
110	6.22×10^{-8}	15.92	389	3.17×10^{-8}	15.68
152	5.29×10^{-8}	15.88	533	2.74×10^{-8}	15.44
208	4.44×10^{-8}	15.88	730	2.11×10^{-8}	15.63
284	4.09×10^{-8}	15.47	999	1.67×10^{-8}	15.66

Mean value of τ_0 is 3.72×10^{-8} s
Mean value of E_a is 15.70 K

V. Computational part

Ab initio calculation

Complete-active-space self-consistent-field (CASSCF) calculations on the individual Dy^{III} or Mn^{III} fragments of **1** and $[Zn_2Dy(L^a)_2Br_2(H_2O)](ClO_4)\cdot 4H_2O$ (**Zn_2Dy**, H_2L^a = *N*,*N*'-bis(3-methoxy-5-methylsalicylidene)-1,2-diaminocyclohexane)[S30] as well as [Dy(bbpen)Br] (**Dy-SIM**, H2bbpen = *N*,*N*'-bis(2-hydroxybenzyl)-*N*,*N*'-bis(2-methylpyridyl)ethylenediamine)[S31] were performed with OpenMolcas and SINGLE_ANISO programs.[S32-S34] Normally, the Dy^{III} or Mn^{III} fragments were constructed based on the single-crystal structure of the computational complexes. However, for **1**, its structure is too large to calculate on our computer. Therefore, we only retained four or three metal ions and the corresponding ligands linking these metal ions in the crystal structure of **1**, while other metal ions and ligands were deleted (Figures S12-S13). Even so, the calculated results from POLY_ANISO are almost consistent with the experimental data, indicating the constructed fragments in this work is reasonable. For each fragment, only one Dy^{III} or Mn^{III} were retained, while other Dy^{III} or Mn^{III} ions were replaced by Lu^{III} or Sc^{III}, respectively. For **Zn_2Dy** and **Dy-SIM**, their crystal structures were directly employed for CASSCF calculations as both complexes contain only one Dy^{III}.

The basis sets for all atoms are atomic orbitals from the ANO-RCC library: ANO-RCC-VTZP for Dy^{III} or Mn^{III}; ANO-RCC-vtz for coordinated N/O atoms; ANO-RCC-vdz for other N/O atoms, Br atoms, Cl atoms, Lu^{III}, Sc^{III}, C and H atoms.[S35] The calculations employed the second order Douglas-Kroll-Hess Hamiltonian, where scalar relativistic contractions were taken into account in the basis set and the spin-orbit couplings were handled separately in the restricted active space interaction (RASSI-SO) procedure.[S36] In the case of the Dy^{III} ion, the active space was defined as nine electrons in seven f orbitals, CAS(9,7). For the CASSCF calculations, the restricted-active-space self-consistent-field (RASSCF) method was employed with the following numbers of multiplets: 21 sextets, 224 quartets and 490 doublets. However, due to the limit of our computer, we only selected 21 sextets, 128 quartets and 130 doublets for the RASSI-SO calculations. In the case of the Mn^{III}, the active space was defined as four electrons in five d orbitals, CAS(4,5). We considered 5 quintets and 45 triplets for RASSCF calculations and employed all of the states for RASSI-SO calculations. Based on the above CASSCF/RASSI-SO calculations, SINGLE_ANISO program was then employed for obtaining the energy levels,[S33-S34] ***g*** tensors, m_J values, magnetic axes, *et al.*

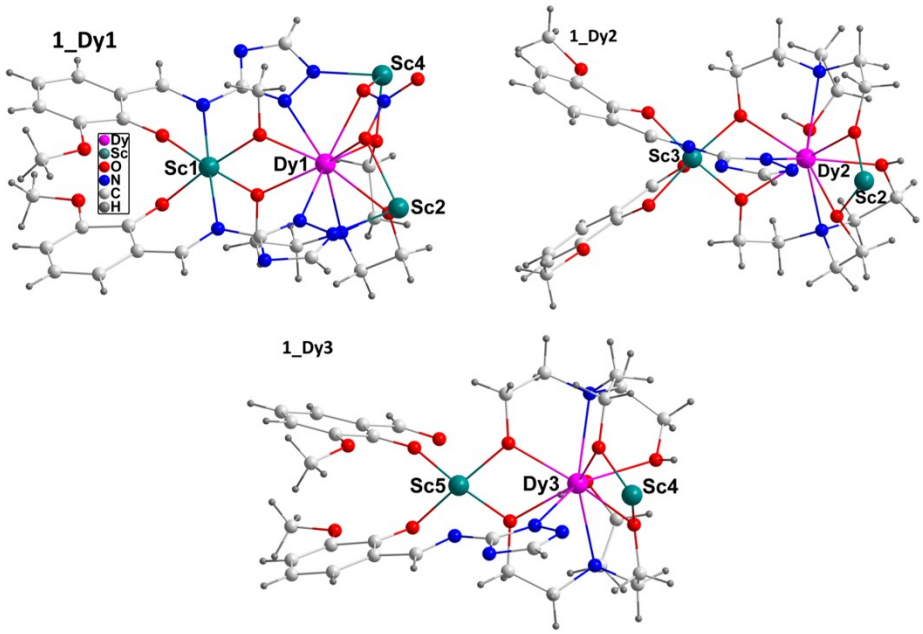

Figure S12. The models for calculating **1_Dy1**, **1_Dy2** and **1_Dy3** in **1**, in which the metal ions were labelled according to the labels on the metal ions in the crystal structure of **1** (see Fig 1).

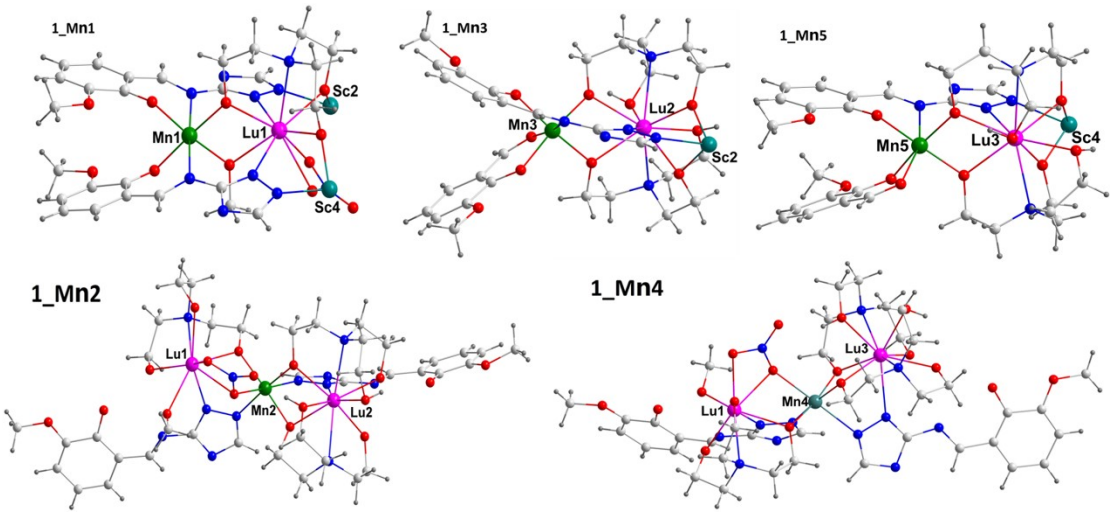

Figure S13. The models of **1_Mn1** ~ **1_Mn5** in **1**, in which the metal ions were labelled according to the labels on the metal ions in the crystal structure of **1** (see Fig 1).

Table S11. Calculated energy levels (cm^{-1}), ***g*** (g_x, g_y, g_z) tensors and predominant m_J values of the lowest eight Kramers doublets (KDs) of individual Dy^{III} fragments, and zero-field splitting parameters D (E) (cm^{-1}), ***g*** (g_x, g_y, g_z) tensors of the lowest spin-orbit states of **1_Mn1**, **1_Mn2**, **1_Mn3, 1_Mn4** and **1_Mn5** for complex **1** using CASSCF/RASSI-SO with OpenMolcas.

KDs	**1_Dy1**			**1_Dy2**			**1_Dy3**		
	E/cm^{-1}	**g**	m_J	E/cm^{-1}	**g**	m_J	E/cm^{-1}	**g**	m_J
1	0.0	0.014 0.016 19.678	±15/2	0.0	0.308 0.952 18.534	±15/2	0.0	0.047 0.114 19.207	±15/2
2	141.3	0.128 0.146 16.358	±13/2	76.4	1.912 2.807 14.964	±1/2	98.4	0.498 0.903 18.091	±1/2
3	296.3	0.756 0.850 13.756	±11/2	133.7	2.424 2.893 12.680	±13/2	143.4	0.187 1.316 15.136	±13/2
4	431.4	1.848 3.184 10.772	±5/2	248.4	2.536 5.858 11.369	±5/2	245.0	2.670 3.109 12.080	±11/2
5	542.4	1.130 3.775 7.996	±7/2	279.0	0.885 4.477 12.762	±9/2	295.3	3.843 5.084 9.890	±7/2
6	620.8	4.335 5.407 8.685	±1/2	331.1	2.706 3.068 12.361	±5/2	352.5	1.243 1.999 13.671	±5/2
7	700.5	1.201 2.648 14.449	±3/2	402.5	0.241 0.321 16.423	±9/2	448.0	0.084 0.101 16.781	±1/2
8	781.9	0.191 0.644 18.283	±1/2	487.6	0.042 0.094 19.450	±3/2	579.3	0.009 0.018 19.582	±5/2

1_Mn1		**1_Mn2**		**1_Mn3**		**1_Mn4**	
D (E)	**g**	D (E)	**g**	D (E)	**g**	D (E)	**g**
-3.4(0.04)	1.995 1.994 1.968	–3.3 (0.1)	1.996 1.994 1.968	–3.4 (0.2)	1.995 1.993 1.966	-3.3(0.2)	1.996 1.994 1.969

1_Mn5	
D (E)	**g**
–3.3 (0.1)	1.995 1.993 1.968

Table S12. Wave functions with definite projection of the total moment | m_J> for the lowest eight KDs of **1_Dy1**, **1_Dy1** and **1_Dy3** using CASSCF/RASSI-SO with OpenMolcas.

	E/cm^{-1}	wave functions
1_Dy1	0.0	96.8%|±15/2>
	141.3	93.7%|±13/2> + 3.0%|±9/2>
	296.3	69.1%|±11/2> + 14.7%|±9/2> + 4.4%|±1/2> + 3.9%|±5/2>
	431.4	15.9%|±5/2> + 15.0%|±3/2> + 12.1%|±7/2> + 10.8%|±1/2> +9.5%|±11/2>
	542.4	43.8%|±7/2> + 19.0%|±9/2> + 11.5%|±3/2> + 9.6%|±1/2> + 8.4%|±5/2>
	620.8	32.1%|±1/2> + 30.7%|±5/2> + 11.0%|±7/2> + 10.7%|±9/2> +10.6%|±3/2> + 4.5%|±11/2>
	700.5	53.2%|±3/2> + 25.3%|±5/2> + 22.3%|±3/2> + 10.0%|±1/2> + 6.4%|±9/2>
	781.9	32.8%|±1/2> + 28.0%|±7/2> + 15.4%|±5/2> + 12.9%|±9/2> + 5.8%|±3/2>
1_Dy2	0.0	83.8%|±15/2> + 10.0%|±11/2>
	76.4	29.5%|±1/2> + 21.0%|±3/2> + 18.1%|±5/2> + 12.3%|±13/2> +9.3%|±9/2> + 4.6%|±7/2> + 3.9%|±15/2>
	133.7	50.9%|±13/2> + 9.4%|±11/2> + 9.3%|±3/2> + 9.1%|±7/2> + 8.4%|±9/2> + 8.2%|±1/2>
	248.4	22.6%|±5/2> + 20.0%|±13/2> + 14.9%|±3/2> + 14.7%|±7/2> + 14.2%| ±11/2> + 7.5%|±9/2>
	279.0	26.7%|±9/2> + 25.7%|±11/2> + 19.2%|±7/2> + 9.1%|±1/2 + 9.1%|±13/2> + 4.3%|±5/2> + 3.7%|±3/2>
	331.1	25.6%|±5/2> + 20.7%|±11/2> + 17.2%|±7/2> + 15.0%|±3/2> + 7.9%| ±1/2> + 6.7%|±9/2>4.7%|±13/2>
	402.5	32.2%|±9/2> + 18.6%|±1/2> + 17.6%|±11/2> + 15.2%|±7/2> + 9.5% |±3/2> + 3.5%|±5/2>
	487.6	25.2%|±3/2> + 24.2%|±5/2> + 22.6%|±1/2> + 17.6%|±7/2> + 8.6%|±9/2>
1_Dy3	0.0	89.3%|±15/2> + 9.0%|±11/2>
	98.4	29.7%|±1/2> + 23.7%|±3/2> + 17.8%|±5/2> + 10.1%|±9/2> + 9.1%|±7/2> + 6.4%|±> + 7.3%|±13/2>
	143.4	76.4%|±13/2> + 5.9%|±11/2> + 5.5%|±7/2> + 4.3%|±9/2> + 3.4%|±1/2> + 3.0%|±> + 2.6%|±13/2>
	245.0	36.8%|±11/2> + 22.4%|±9/2> + 12.0%|±3/2> + 9.7%|±5/2> + 9.5%|±1/2> + 4.7%|±7/2> + 3.1%|±15/2>
	295.3	31.8%|±7/2> + 16.0%|±11/2> + 15.7%|±9/2> + 12.8%|±5/2> + 8.1% |±1/2> + 7.7%|±3/2> + 5.8%|±13/2>
	352.5	29.9%|±5/2> + 18.2%|±3/2> + 14.9%|±7/2> + 14.3%|±11/2> + 12.3% |±9/2> + 4.7%|±13/2> + 4.0%|±1/2>
	448.0	27.3%|±1/2> + 14.7%|±3/2> + 13.1%|±11/2> + 12.5%|±7/2> + 10.0% |±9/2> + 5.7%|±5/2> + 2.6%|±13/2>
	579.3	23.1%|±5/2> + 21.0%|±3/2> + 20.8%|±7/2> + 17.7%|±1/2> + 12.4% |±9/2> + 3.4%|±11/2>

Table S13. Calculated spin-free energies (cm^{-1}) of the lowest ten terms of **1_Mn1, 1_Mn2, 1_Mn3, 1_Mn4 and 1_Mn5 for complex 1** using CASSCF with OpenMolcas.

KDs	**1_Mn1** E/cm^{-1}	**1_Mn2** E/cm^{-1}	**1_Mn3** E/cm^{-1}	**1_Mn4** E/cm^{-1}	**1_Mn5** E/cm^{-1}
1	0.0	0.0	0.0	0.0	0.0
2	11922.2	13701.95	11722.3	13882.3	12961.6
3	18015.0	18256.34	17374.2	18559.9	17932.0
4	20352.2	21633.38	20019.9	21514.3	19856.7
5	20729.1	21941.51	20346.6	22325.3	20323.7
6	16749.3	17501.49	17129.5	17258.4	18324.2
7	17376.0	17715.65	17329.3	17862.2	18644.3
8	18582.5	19930.48	18950.5	19770.3	19579.7
9	22968.8	23045.09	23091.6	23032.2	23123.3
10	25339.6	25853.29	25573.3	25834.7	25704.8

Table S14. Calculated weights of the five most important spin-free states for the lowest five spin-orbit states from **1_Mn1** to **1_Mn5 for complex 1** using CASSCF/RASSI-SO with OpenMolcas.

	Spin-orbit states	Energy (cm^{-1})	Spin-free states, Spin, Weights				
1_Mn1	1	0.0	1,2.0,0.9987	3,2.0,0.0004	6,1.0,0.0003	7,1.0,0.0002	19,1.0,0.0001
	2	0.0	1,2.0,0.9987	3,2.0,0.0004	6,1.0,0.0003	7,1.0,0.0002	19,1.0,0.0001
	3	10.0	1,2.0,0.9993	6,1.0,0.0002	3,2.0,0.0001	7,1.0,0.0001	4,2.0,0.0001
	4	10.3	1,2.0,0.9993	7,1.0,0.0001	3,2.0,0.0001	6,1.0,0.0001	19,1.0,0.0001
	5	13.6	1,2.0,0.9995	6,1.0,0.0001	7,1.0,0.0001	15,1.0,0.0001	5,2.0,0.0001
1_Mn2	1	0.0	1,2.0,0.9988	3,2.0,0.0004	6,1.0,0.0002	7,1.0,0.0002	19,1.0,0.0001
	2	0.0	1,2.0,0.9988	3,2.0,0.0004	6,1.0,0.0002	7,1.0,0.0002	19,1.0,0.0001
	3	9.7	1,2.0,0.9993	6,1.0,0.0001	7,1.0,0.0001	3,2.0,0.0001	5,2.0,0.0001
	4	10.3	1,2.0,0.9994	6,1.0,0.0001	7,1.0,0.0001	3,2.0,0.0001	19,1.0,0.0001
	5	13.3	1,2.0,0.9995	6,1.0,0.0001	7,1.0,0.0001	15,1.0,0.0001	5,2.0,0.0000
1_Mn3	1	0.0	1,2.0,0.9987	3,2.0,0.0004	6,1.0,0.0003	7,1.0,0.0002	19,1.0,0.0001
	2	0.1	1,2.0,0.9987	3,2.0,0.0004	6,1.0,0.0003	7,1.0,0.0002	20,1.0,0.0001
	3	9.8	1,2.0,0.9993	6,1.0,0.0003	3,2.0,0.0001	4,2.0,0.0001	19,1.0,0.0001
	4	10.9	1,2.0,0.9993	7,1.0,0.0002	3,2.0,0.0001	20,1.0,0.0001	5,2.0,0.0001
	5	13.8	1,2.0,0.9995	7,1.0,0.0001	6,1.0,0.0001	15,1.0,0.0001	4,2.0,0.0001
1_Mn4	1	0.0	1,2.0,0.9988	3,2.0,0.0004	6,1.0,0.0003	7,1.0,0.0002	16,1.0,0.0001
	2	0.0	1,2.0,0.9988	3,2.0,0.0004	6,1.0,0.0003	7,1.0,0.0002	18,1.0,0.0001
	3	9.4	1,2.0,0.9993	6,1.0,0.0002	3,2.0,0.0001	4,2.0,0.0001	16,1.0,0.0001
	4	10.5	1,2.0,0.9994	7,1.0,0.0002	3,2.0,0.0001	18,1.0,0.0001	5,2.0,0.0001
	5	13.3	1,2.0,0.9995	7,1.0,0.0001	6,1.0,0.0001	15,1.0,0.0001	4,2.0,0.0001
1_Mn5	1	0.0	1,2.0,0.9988	3,2.0,0.0004	6,1.0,0.0002	7,1.0,0.0002	16,1.0,0.0001
	2	0.0	1,2.0,0.9988	3,2.0,0.0004	6,1.0,0.0002	7,1.0,0.0002	16,1.0,0.0001
	3	9.5	1,2.0,0.9993	6,1.0,0.0002	3,2.0,0.0001	4,2.0,0.0001	16,1.0,0.0001
	4	10.2	1,2.0,0.9994	7,1.0,0.0002	3,2.0,0.0001	5,2.0,0.0001	17,1.0,0.0001
	5	13.2	1,2.0,0.9995	15,1.0,0.0001	7,1.0,0.0001	4,2.0,0.0001	6,1.0,0.0001

Table S15. Calculated energy levels (cm^{-1}), ***g*** (g_x, g_y, g_z) tensors and predominant m_J values of the lowest eight Kramers doublets (KDs) for **Zn_2Dy** and **Dy-SIM** complexes using CASSCF/RASSI-SO with OpenMolcas.

KDs	**Zn_2Dy**			**Dy-SIM**		
	E/cm^{-1}	**g**	m_J	E/cm^{-1}	**g**	m_J
1	0.0	0.003 0.004 19.736	±15/2	0.0	0.0006 0.0007 19.879	±15/2
2	191.8	0.035 0.051 17.157	±13/2	393.6	0.064 0.083 16.980	±1/2
3	323.0	0.298 0.480 14.179	±11/2	626.2	0.898 1.598 13.487	±13/2
4	397.2	1.134 2.036 11.432	±9/2	720.0	4.839 5.998 9.747	±5/2
5	461.5	1.644 2.028 16.322	±7/2	781.2	1.204 3.824 10.047	±9/2
6	496.3	7.795 5.997 0.035	±3/2	799.4	0.918 4.582 13.008	±5/2
7	577.1	2.543 3.988 13.191	±1/2	806.4	0.141 0.269 16.944	±9/2
8	680.7	0.410 1.449 18.144	±3/2	876.1	0.143 0.203 18.489	±3/2

Table S16. Wave functions with definite projection of the total moment | m_J> for the lowest eight KDs of Dy in **Zn_2Dy** and **Dy-SIM** complexes using CASSCF/RASSI-SO with OpenMolcas.

	E/cm^{-1}	wave functions
Zn_2Dy	0.0	97.6%|±15/2>
	191.8	88.0%|±13/2> + 6.9%|±11/2>
	323.0	73.9%|±11/2> + 9.5%|±7/2> + 7.9%|±13/2> + 6.0%|±9/2>
	397.2	68.8%|±9/2> + 16.5%|±5/2> + 6.5%|±7/2> + 3.3%|±13/2> +2.5%|±11/2>
	461.5	53.4%|±7/2> + 15.2%|±5/2> + 12.8%|±11/2> + 12.7%|±9/2> + 3.5%|±1/2>
	496.3	43.5%|±3/2> + 24.1%|±5/2> + 19.5%|±7/2> + 8.4%|±1/2> + 4.2%|±9/2>
	577.1	54.1%|±1/2> + 25.1%|±5/2> + 14.0%|±3/2> + 4.1%|±7/2> + 2.5%|±9/2>
	680.7	38.6%|±3/2> + 33.2%|±1/2> + 19.7%|±5/2> + 6.7%|±7/2> + 1.5%|±9/2>
Dy-SIM	0.0	99.6%|±15/2>
	393.6	99.0%|±13/2> + 0.6%|±9/2>
	626.2	90.1%|±11/2> + 5.6%|±7/2> + 2.3%|±1/2> + 0.8%|±5/2> + 0.8%|±3/2>
	720.0	44.9%|±9/2> + 21.8%|±5/2> + 16.7%|±3/2> + 6.5%|±1/2> + 5.3%| ±7/2> + 4.3%| ±11/2>
	781.2	34.9%|±1/2> + 33.4%|±9/2> + 15.6%|±7/2> + 11.8%|±3/2> + 2.6%|±11/2> + 1.1%|±5/2
	799.4	45.2%|±1/2> + 33.5%|±9/2> + 25.9%|±3/2> + 16.1%|±7/2> + 2.6%| ±11/2>
	806.4	38.9%|±5/2> + 27.8%|±3/2> + 23.4%|±7/2> + 3.0%|±9/2> + 6.5% |±1/2>
	876.1	34.9%|±5/2> + 31.4%|±7/2> + 16.9%|±3/2> + 10.6%|±9/2> + 4.3%|±1/2> + 1.7%|±11/2>

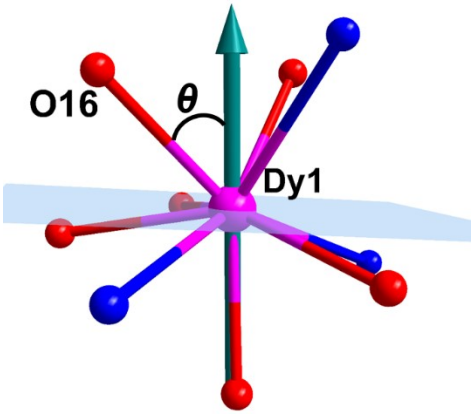

Figure S14. The plot shown the mean of θ, employing Dy1-O16 as an example. The teal arrow represents the direction of the main magnetic axis of Dy1 calculated by OpenMolcas.

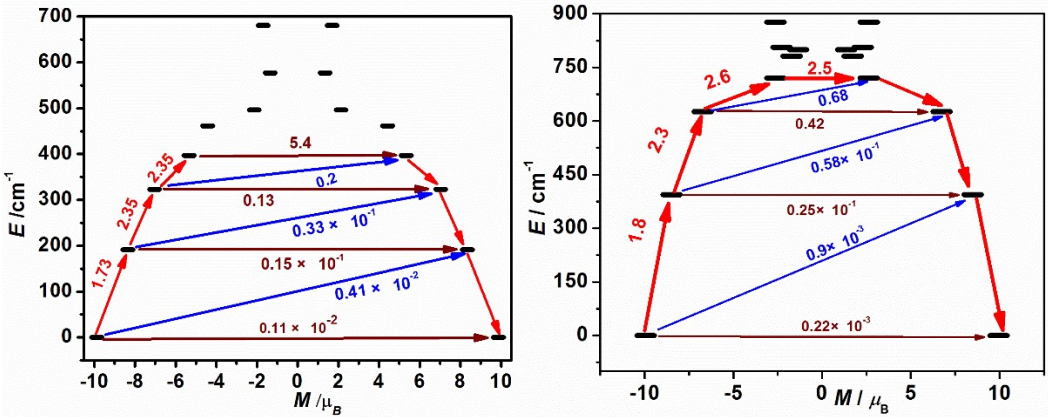

Figure S15. Magnetization blocking barriers for individual fragments of **Zn_2Dy** (left) and **Dy-SIM** (right) obtained by SINGLE_ANISO calculations. The red lines represent the QTM process, while the blue/violet lines represent the Orbach/Raman processes. The numbers near the paths are averaged transition moments in μ_B, connecting the corresponding states.

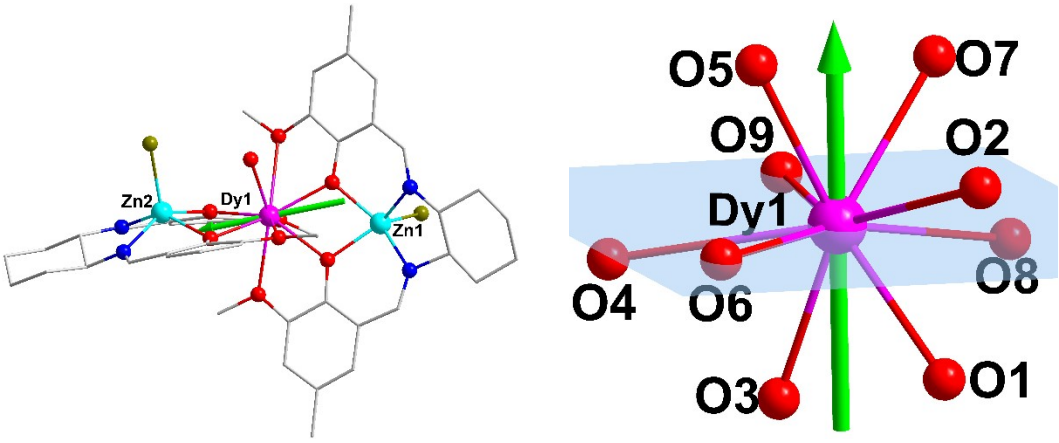

Figure S16. Calculated orientations of the local magnetic axes on Dy^{III} for complex **Zn_2Dy** in its ground KDs. The main axes and the equatorial sites of Dy1 were shown by green arrows and by blue planes, respectively.

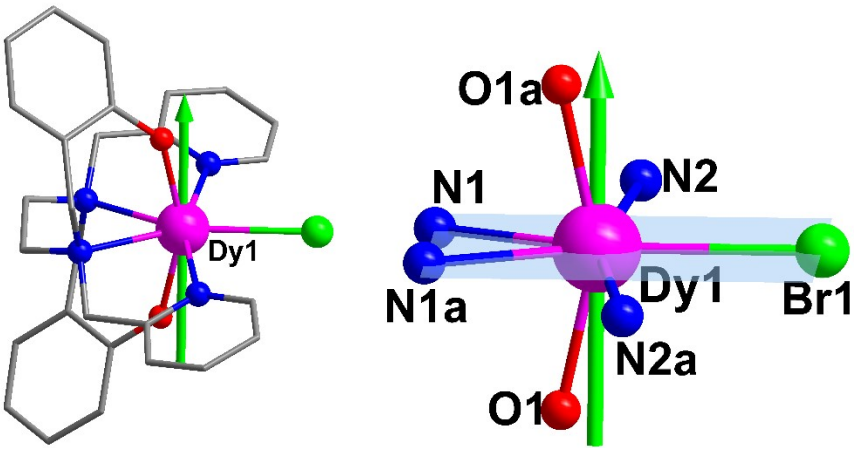

Figure S17. Calculated orientations of the local magnetic axes on Dy^{III} for complex **Dy-SIM** in its ground KDs. The main axes and the equatorial sites of Dy1 were shown by green arrows and by blue planes, respectively.

Table S17. The details for analyzing the relationship among the U_{cal} values of **1_Dy1 ~ 1_Dy3** in **1**, and Dy fragments in **Zn_2Dy** complex as well as in **Dy-SIM** complex, the Dy-O or Dy-N bond lengths as well the θ angles.

Bonds	Bond lengths	θ_i or θ_j	$\sin\theta_{i(j)}$	$\cos\theta_{i(j)}$	R_{eq}[a]	R_{ax}[b]	U_{cal} (cm^{-1})
			1				
Dy1-O15	2.298	113.956	0.9139	-0.4060			
Dy1-O16	2.38	48.515	0.7491	0.6624			
Dy1-O17	2.433	41.484	0.6624	0.7491			
Dy1-O30	2.377	94.344	0.9971	-0.0757			
Dy1-O31	2.435	99.698	0.9857	-0.1685	17.99	-0.25	296.17
Dy1-O33	2.328	161.142	0.3232	-0.9463			
Dy1-N2	2.555	105.369	0.9642	-0.2650			
Dy1-N6	2.604	110.280	0.9380	-0.3466			
Dy1-N17	2.649	51.331	0.7808	0.6248			
Dy2-O18	2.336	68.413	0.9299	0.3679			
Dy2-O19	2.477	70.522	0.9428	0.3334			
Dy2-O20	2.396	141.323	0.6249	-0.7807			
Dy2-O21	2.321	79.144	0.9821	0.1883			
Dy2-O22	2.437	5.474	0.0954	0.9954	17.40	0.34	76.45
Dy2-O23	2.291	125.647	0.8126	-0.5828			
Dy2-N10	2.660	134.425	0.7142	-0.7000			
Dy2-N18	2.605	84.858	0.9960	0.0896			
Dy2-N19	2.604	76.044	0.9705	0.2412			
Dy3-O24	2.302	118.212	0.8812	-0.4727			
Dy3-O25	2.359	26.677	0.4490	0.8936			
Dy3-O26	2.492	116.491	0.8950	-0.4461			
Dy3-O27	2.412	106.431	0.9592	-0.2829			
Dy3-O28	2.424	162.248	0.3049	-0.9524	16.28	-0.76	98.39
Dy3-O29	2.323	31.809	0.5271	0.8498			
Dy3-N14	2.601	42.983	0.6818	0.7316			
Dy3-N20	2.625	98.771	0.9883	-0.1525			
Dy3-N21	2.586	116.607	0.8941	-0.4479			
			Zn_2Dy				
Dy1-O1	2.321	136.775	0.6849	-0.7287			
Dy1-O2	2.608	49.471	0.7601	0.6498			
Dy1-O3	2.275	167.264	0.2205	-0.9754			
Dy1-O4	2.771	123.847	0.8305	-0.5570			
Dy1-O5	2.303	21.761	0.3707	0.9287	15.69	-0.12	397.25
Dy1-O6	2.538	101.694	0.9792	-0.2027			
Dy1-O7	2.307	25.845	0.4359	0.9000			
Dy1-O8	2.578	87.557	0.9991	0.0426			
Dy1-O9	2.397	94.107	0.9974	-0.0716			
			Dy-SIM				
Dy1-O1	2.163	160.958	0.3263	-0.9453			
Dy1-N1	2.578	101.530	0.9798	-0.1999			
Dy1-N2	2.594	98.081	0.9901	-0.1406	14.45	-5.9×10^{-5}	720.02
Dy1-Br1	2.851	89.993	1.0000	0.0001			
Dy1-O1a	2.163	19.050	0.3264	0.9452			
Dy1-N1a	2.578	78.479	0.9799	0.1997			
Dy1-N2a	2.594	81.918	0.9901	0.1406			

Note:

[a]The equation for calculating the R_{eq} parameter is:

$$R_{eq} = \sum_{i=1}^{n} r_i sin\theta_i + \sum_{j=1}^{l} r_j sin\theta_j$$

[b]The equation for calculating the R_{ax} parameter is:

$$R_{ax} = \sum_{i=1}^{n} r_i cos\theta_i + \sum_{j=1}^{l} r_j cos\theta_j$$

In the two equations, R_{eq} and R_{ax} are the parameters for describing the physical characteristics on the equation plane and along the axial directions of each Dy^{III} in **1**. r_i and r_j represent the bond lengths of Dy-O and Dy-N for each Dy^{III} (i and j are the number of O atoms and N atoms around each Dy^{III}), while θ_i and θ_j represent the angles between Dy-O or Dy-N and the main magnetic axes of each Dy^{III} (see Figure S15).

To fit the intramolecular magnetic interactions between paramagnetic ions in **1**, we taken two steps to obtain them. Firstly, we calculated individual Dy^{III} and Mn^{III} fragments using CASSCF/RASSI-SO to obtain the corresponding magnetic properties. Then, exchange interaction between the magnetic center was considered within the Lines model, which is effective and has been successfully used widely in the research field of d- and f-elements single molecule magnets.[S37-S38] From Figure S15, the magnetic couplings within **1** were extracted using the Hamiltonian:

$$\hat{H}_{exch} = -\tilde{J}_1\hat{S}_{Dy1}\hat{S}_{Mn1} - J_2(\hat{S}_{Dy1}\hat{S}_{Mn2} + \hat{S}_{Dy1}\hat{S}_{Mn4}) - \tilde{J}_3(\hat{S}_{Dy2}\hat{S}_{Mn2} + \hat{S}_{Dy3}\hat{S}_{Mn4}) - \tilde{J}_4(\hat{S}_{Dy2}\hat{S}_{Mn3} - \hat{S}_{Dy3}\hat{S}_{Mn5})$$

In this equation, $\tilde{J}_i$ values are the total magnetic interactions in combination of calculated $\tilde{J}_i^{dipolar}$ and the fitted $\tilde{J}_i^{exch}$ parameters, in which $\tilde{J}_i^{dipolar}$ and $\tilde{J}_i^{exch}$ represent dipolar interactions and exchange coupling interactions, respectively. The Lines exchange couplings were fitted through comparison of the computed[S39] and the experimental magnetic susceptibilities using POLY_ANISO program.[S33-S34,S40]

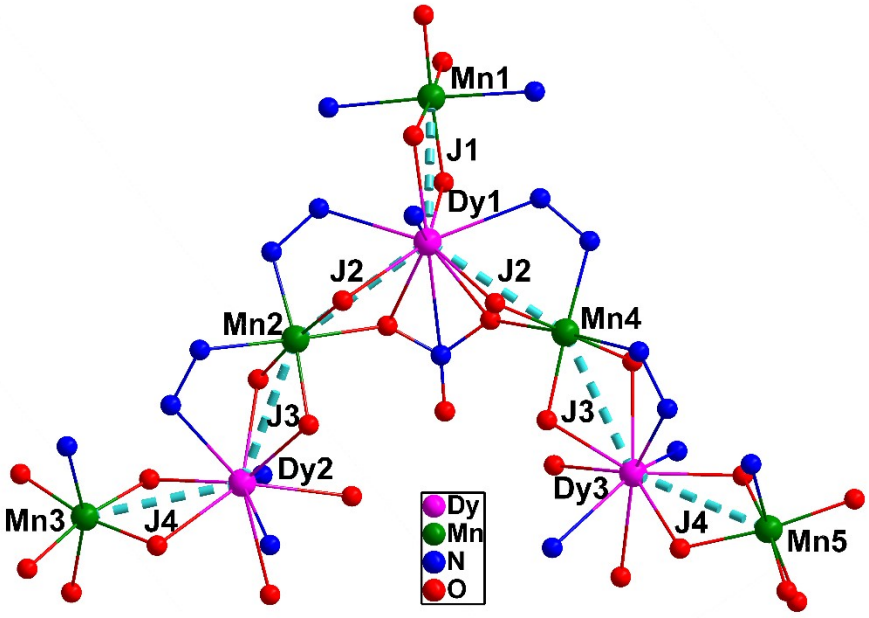

Figure S18. The coupling model for **1**.

Table S18. The details for calculating intramolecular dipole-dipole interaction $\tilde{J}_{dip}$ in **1** by employing the equation of $\tilde{J}_{dip} = -\frac{\mu_B{}^2 g_{1z} g_{2z}}{r^3}(cos\theta - 3cos\varphi_1 cos\varphi_2)$,[S41] in which $\mu_B{}^2$ = 0.4329701512063995 cm^{-1}/T, r is the distances between Mn^{III} and Dy^{III}, θ is the angle between the main magnetic axes of Mn^{III} and Dy^{III}, and φ_1 or φ_2 represent the angles between the main magnetic axis of Mn^{III} or Dy^{III} and $Mn^{III}\cdots Dy^{III}$ lines, respectively.

J_{idip}	g_z of Dy	g_z of Mn	r (Å)	θ (°)	φ_1 (°)	φ_2 (°)	A^* values	J_{dip} values
$\tilde{J}_{1dip}$	19.6779	1.9679	3.340	90.670	161.59	83.353	0.3177	-0.14
$\tilde{J}_{2dip}$	19.6779	1.9687	3.505	85.666	73.072	100.17	0.2165	-0.08
$\tilde{J}_{3dip}$	18.8705	1.9687	3.360	66.751	92.884	87.647	0.8338	-0.36
$\tilde{J}_{4dip}$	18.8705	1.9669	3.412	91.861	97.391	91.647	-0.7741	0.32

Note: 1) $\tilde{J}_{1dip}$, $\tilde{J}_{2dip}$, $\tilde{J}_{3dip}$ and $\tilde{J}_{4dip}$ were calculated by employing Mn1···Dy1, Dy1···Mn2, Mn2···Dy2 and Dy2····Mn3 pairs, respectively. 2) $A^* = cos\theta - 3cos\varphi_1 cos\varphi_2$.

DFT calculations

The density functional theory (DFT) calculations were performed with ORCA 5.0.4 software.[S42-S43] The PBE0 hybrid functional was employed for calculating the isotropic exchange constants *J*,[S44] which were obtained according to the Ruiz's approach by comparing the energies of high-spin (HS) and broken-symmetry (BS) spin states.[S45] The computational model was constructed by replacing the Dy^{III} in the crystal structure of **1** by Gd^{III}. During the calculation, the relativistic effects were included with zero-order regular approximation (ZORA)[S46] together with the scalar relativistic contracted version of the basis functions: zora-def2-TZVP for Mn^{III}, SARC2-zora-QZV for Gd^{III}, zora-def2-TZVP(-f) for O and N atoms, and zora-def2-SVP for C and H atoms.[S47] Additionally, the calculations employed the RI approximation with the def2/J and SARC/J Coulomb fitting basis set as an auxiliary basis set[S48] and the chain-of-spheres (RIJCOSX) approximation to exact exchange implemented in ORCA.[S49] The tight grid (Defgrid3 in ORCA 5.0.4 convention) and the tight self-consistent field convergence criteria (tightscf in ORCA 5.0.4 convention) were employed in all calculations. Notably, when the default value of 0.85 for dampfac parameter in ORCA was employed, the calculations for HS and different BS states can not be converged, so the dampfac value was set to be 0.95.

Table 19. States, derived energies and derived Δ_i for Gd Analogue of **1** by employing the Hamiltonian of $H = -J_1S_{Mn1}S_{Gd1} - J_2(S_{Mn2}S_{Gd1} + S_{Mn4}S_{Gd1}) - J_3(S_{Mn2}S_{Gd2} + S_{Mn4}S_{Gd3}) - J_4(S_{Mn3}S_{Gd2} + S_{Mn5}S_{Gd3})$ (the employed mode shown in Figure S15).

States	Derived energies	Derived Δ_i ($\Delta_i = E_{BSi} - E_{HS}$)
Mn1Gd1Mn2Gd2Mn3Mn4Gd3Mn5	$E_{HS} = -\frac{143}{4}J_1 - \frac{143}{2}J_2 - \frac{143}{2}J_3 - \frac{143}{2}J_4$	
Gd1Mn2Gd2Mn3Mn4Gd3Mn5	$E_{BS1} = -\frac{15}{4}J_1 - \frac{143}{2}J_2 - \frac{143}{2}J_3 - \frac{143}{2}J_4$	$\Delta_1 = 32J_1$
Gd1Gd2Mn3Mn4Gd3Mn5	$E_{BS2} = -\frac{15}{4}J_1 - \frac{158}{4}J_2 - \frac{158}{4}J_3 - \frac{143}{2}J_4$	$\Delta_2 = 32J_1 + 32J_2 + 32J_3$
Mn1Mn2Gd2Mn3Mn4Gd3Mn5	$E_{BS3} = -\frac{15}{4}J_1 - \frac{15}{2}J_2 - \frac{143}{2}J_3 - \frac{143}{2}J_4$	$\Delta_3 = 32J_1 + 64J_2$
Gd1Gd2Gd3	$E_{BS4} = -\frac{15}{4}J_1 - \frac{15}{2}J_2 - \frac{15}{2}J_3 - \frac{15}{2}J_4$	$\Delta_4 = 32J_1 + 64J_2 + 64J_3 + 64J_4$

From the energy data in Table S19, we can obtain the J_i as follows:

$$J_1 = \frac{\Delta_1}{32}; \quad J_2 = \frac{\Delta_3 - \Delta_1}{64}; \quad J_3 = \frac{2\Delta_2 - \Delta_1 - \Delta_3}{64}; \quad J_4 = \frac{\Delta_4 - 2\Delta_2 + \Delta_1}{64}$$

Table S20. The information for HS state and different BS states calculated from the DFT calculations for Gd Analogue of **1**.

States	Energies (Eh)	S^2	Calculated Δ_i (Eh)
HS	-47454.851267	440.9894	
BS1	-47454.851388	292.9888	-0.000121
BS2	-47454.852072	176.9844	-0.000805
BS3	-47454.851449	202.9882	-0.000182
BS4	-47454.851740	20.9871	-0.000473

From Table S20, the calculated J_i (1 Eh = 219474.63137 cm^{-1}) are: $J_1 = -0.83$ cm^{-1}, $J_2 = -0.21$ cm^{-1}, $J_3 = -4.48$ cm^{-1}, $J_4 = 3.48$ cm^{-1}.

VI. References

References

S1. C. Papatriantafyllopoulou, W. Wernsdorfer, K. A. Abboud, G. Christou, *Inorg. Chem.* **2011**, *50*, 421–423.

S2. J. L. Liu, F. S. Guo, Z. S. Meng, Y. Z. Zheng, J. D. Leng, M. L. Tong, L. Ungur, L. F. Chibotaru, K. J. Herouxc, D. N. Hendrickson, *Chem. Sci*. **2011**, *2*, 1268–1272.

S3. S. F. M. Schmidt, M. P. Merkel, G. E. Kostakis, G. Buth, C. E. Ansona, A. K. Powell, *Dalton Trans.* **2017**, *46*, 15661−15665.

S4. V. Mereacre, A. M. Ako, R. Clérac, W. Wernsdorfer, I. J. Hewitt, C. E. Anson, A. K. Powell, *Chem. Eur. J.* **2008**, *14*, 3577–3584.

S5. Y. Peng, M. K. Singh, V. Mereacre, C. E. Anson, G. Rajaraman, A. K. Powell, *Chem. Sci*. **2019**, *10*, 5528–5538.

S6. P. Bag, A. Chakraborty, G. Rogez, V. Chandrasekhar, *Inorg. Chem.* **2014**, *53*, 6524–6533.

S7. M. Darii, V. Ch. Kravtsov, K. Krämer, J. Hauser, S. Decurtins, S. X. Liu, M. Affronte, S. G. Baca, *Cryst. Growth Des.* **2020**, *20*, 1, 33–38.

S8. M. M. Hänninen, A. J. Mota, R. Sillanpää, S. Dey, G. Velmurugan, G. Rajaraman, E. Colacio, *Inorg. Chem.* **2018**, *57*, 3683–3698.

S9. V. Chandrasekhar, P. Bag, M. Speldrich, J. van Leusen, P. Kögerler, *Inorg. Chem*. **2013**, *52*, 5035-5044.

S10. K. N. Pantelis, K. H. Baka, J. Huang, C. P. Raptopoulou, V. Psycharis, K. R. Dunbar, T. C. Stamatatos, *Cryst. Growth Des*. **2023**, *23*, 5301-5313.

S11. K. R. Vignesh, S. K. Langley, B. Moubaraki, K. S. Murray, G. Rajaraman, *Inorg. Chem.* **2018**, *57*, 1158-1170.

S12. H. Chen, C. B. Ma, M. Q. Hu, H. M. Wen, C. N. Chen, *Dalton Trans*. **2014**, *43*, 16737–16744.

S13. H. S. Wang, Y. Chen, Z. B. Hu, K. Zhang, Z. Zhang, Y. Song, Z. Q. Pan, *New J. Chem.* **2020**, *44*, 16302−16310.

S14. MSavva, K. Skordi, A. D. Fournet, A. E. Thuijs, G. Christou, S. P. Perlepes, C. Papatriantafyllopoulou, A. J. Tasiopoulos, *Inorg. Chem.* **2017**, *56*, 5657-5668.

S15. D. I. Alexandropoulos, T. N. Nguyen, L. Cunha-Silva, T. F. Zafiropoulos, A. Escuer, G. Christou, T. C. Stamatatos, *Inorg. Chem*. **2013**, *52*, 1179-1181.

S16. V. Mereacre, M. N. Akhtar, Y. Lan, A. M. Ako, R. Clérac, C. E. Anson, A. K. Powell, *Dalton Trans.* **2010**, *39*, 4918-4927.

S17. P. Hu, X. Wang, C. Jiang, F. Yu, B. Li, G. Zhuang, T. Zhang, *Inorg. Chem.* **2018**, *57*, 8639–8645.

S18. T. G. Tziotzi, D. I. Tzimopoulos, T. Lis, R. Inglis, C. J. Milios, *Dalton Trans*. **2015**, *44*, 11696-11699.

S19. S. Yu, H. Hu, H. H. Zou, D. Liu, Y. Liang, F. P. Liang, Z. Chen, *Inorg. Chem*. **2022**, *61*, 3655-3663.

S20. M. Darii, J. van Leusen, V. Ch. Kravtsov, Y. Chumakov, K. Kramer, S. Decurtins, S. X. Liu, P. Kogerler, S. G. Baca, *Cryst. Growth Des*. **2023**, *23*, 6944-6952.

S21. H. S. Wang, F. J. Yang, Q. Q. Long, Z. Y. Huang, W. Chen, Z. Q. Pan, Y. Song, *Dalton Trans*. **2016**, *45*, 18221-18228.

S22. K. R. Vignesh, S. K. Langley, B. Moubaraki, K. S. Murray, G. Rajaraman, *Chem. Eur. J.*

2015, *21*, 16364-16369.

S23. A. M. Ako, V. Mereacre, R. Clérac, W. Wernsdorfer, I. J. Hewitt, C. E. Anson, A. K. Powell, *Chem. Commun*. **2009**, 544-546.

S24. S. H. Sumrraa, A. Sulemana, Z. H. Chohanb, M. N. Zafarc, M. A. Razaa, T. Iqba, *Russ. J. Gen. Chem*. **2017**, *87*, 1281−1287.

S25. *SAINT Plus, v. 7.03*; Bruker AXS Inc: 2004.

S26. G. M. Sheldrick, SADABS: Program for Empirical Absorption Correction of Area Detector Data; University of Göttingen: 1996.

S27. G. M. Sheldrick, Acta Crystallogr., Sect. A: Found. Crystallogr. **2008**, 64, 112−122.

S28. A. Spek, *J. Appl. Crystallogr*. **2003**, *36*, 7−13.

S29. G. A. Bain, J. F. Berry, *J. Chem. Educ*. **2008**, *85*, 532−536.

S30. R. Nandy, Z. Jagličić, N. Ch. Jana, P. Brandão, F. Bustamante, D. Aravena, A. Panja, *Dalton Trans*. **2024**, *53*, 13968-13981.

S31. J. Liu, Y. C. Chen, J. L. Liu, V. Vieru, L. Ungur, J. H. Jia, L. F. Chibotaru, Y. Lan, W. Wernsdorfer, S. Gao, X. M. Chen, M. L. Tong, *J. Am. Chem. Soc*. **2016**, *138*, 5441-5450.

S32. I. Fdez. Galván, M. Vacher, A. Alavi, C. Angeli, F. Aquilante, J. Autschbach, J. J. Bao, S. I. Bokarev, N. A. Bogdanov, R. K. Carlson, L. F. Chibotaru, J. Creutzberg, N. Dattani, M. G. Delcey, S. S. Dong, A. Dreuw, L. Freitag, L. M. Frutos, L. Gagliardi, F. Gendron, A. Giussani, L. González, G. Grell, M. Guo, C. E. Hoyer, M. Johansson, S. Keller, S. Knecht, G. Kovačević, E. Källman, G. Li Manni, M. Lundberg, Y. Ma, S. Mai, J. P. Malhado, P. Å. Malmqvist, P. Marquetand, S. A. Mewes, J. Norell, M. Olivucci, M. Oppel, Q. M. Phung, K. Pierloot, F. Plasser, M. Reiher, A. M. Sand, I. Schapiro, P. Sharma, C. J. Stein, L. K. Sørensen, D. G. Truhlar, M. Ugandi, L. Ungur, A. Valentini, S. Vancoillie, V. Veryazov, O. Weser, T. A. Wesołowski, P. O. Widmark, S. Wouters, A. Zech, J. P. Zobel, R. Lindh, *J. Chem. Theory Comput*. **2019**, *15*, 5925−5964.

S33. L. F. Chibotaru, L. Ungur, A. Soncini, *Angew. Chem., Int. Ed*. **2008**, *47*, 4126−4129.

S34. L. F. Chibotaru, L. Ungur, C. Aronica, H. Elmoll, G. Pilet, D. Luneau, *J. Am. Chem. Soc*. **2008**, *130*, 12445−12455.

S35. B. O. Roos, R. Lindh, P. Å. Malmqvist, V. Veryazov, P. O. Widmark, *Chem. Phys. Lett*. **2005**, *409*, 295-299.

S36. B. A. Heß, C. M. Marian, U. Wahlgren, O. A. Gropen, *Chem. Phys. Lett*. **1996**, *251*, 365-371.

S37. K. C. Mondal, A. Sundt, Y. H. Lan, G. E. Kostakis, O. Waldmann, L. Ungur, L. F. Chibotaru, C. E. Anson, A. K. Powell, *Angew. Chem., Int. Ed.* **2012**, *51*, 7550−7554.

S38. S. K. Langley, D. P. Wielechowski, V. Vieru, N. F. Chilton, B. Moubaraki, B. F. Abrahams, L. F. Chibotaru, K. S. Murray, *Angew. Chem., Int. Ed.* **2013**, *52*, 12014–12019.

S39. M. E. Lines, *J. Chem. Phys*. **1971**, *55*, 2977−2984.

S40. L. Ungur, W. Van den Heuvel, L. F. Chibotaru, *New J. Chem*. **2009**, *33*, 1224−1230.

S41. P. Panissod, M. Drillon, *In Magnetism Molecules to Materials IV*; Miller, J. S., Drillon, M., Ed.; Wiley-VCH Verlag GmbH & Co. KGaA, 2002; Chapter 7, p325.

S42. F. Neese, *Wiley Interdiscip. Rev.: Comput. Mol. Sci*. **2012**, *2*, 73-78.

S43. F. Neese, *Wiley Interdiscip. Rev. Comput. Mol. Sci*. **2018**, *8*, No. e1327.

S44. C. Adamo, V. Barone, *J. Chem. Phys*. **1999**, *110*, 6158-6170.

S45. E. Ruiz, A. Rodríguez-Fortea, J. Cano, S. Alvarez, P. Alemany, *J. Comput. Chem*. **2003**, *24*, 982-989.

S46. E. v. Lenthe, E. J. Baerends, J. G. Snijders, *J. Chem. Phys*. **1993**, *99*, 4597-4610.
S47. D. A. Pantazis, X.-Y. Chen, C. R. Landis, F. Neese, *J. Chem. Theory Comput*. **2008**, *4*, 908-919.
S48. G. L. Stoychev, A. A. Auer, F. Neese, *J. Chem. Theory Comput*. **2017**, *13*, 554-562.
S49. R. Izsak, F. Neese, *J. Chem. Phys*. **2011**, *135*, 144105.